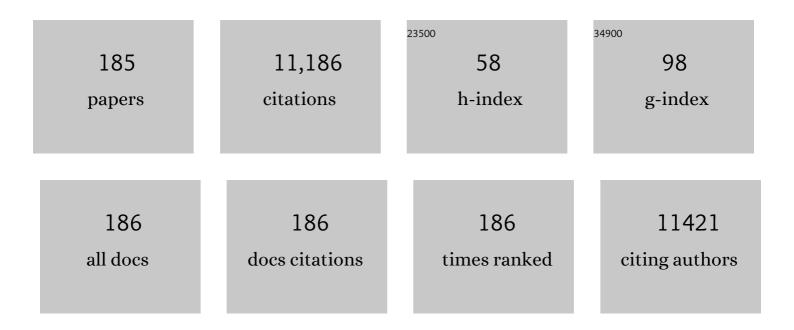
Liqiang Jing

List of Publications by Year in descending order

Source: https://exaly.com/author-pdf/3922813/publications.pdf Version: 2024-02-01



#	Article	IF	CITATIONS
1	Comparative study of metal oxides and phosphate modification with different mechanisms over g-C3N4 for visible-light photocatalytic degradation of metribuzin. Rare Metals, 2022, 41, 155-165.	3.6	50
2	A novel composite anode via immobilizing of Ce-doped PbO2 on CoTiO3 for efficiently electrocatalytic degradation of dye. Journal of Colloid and Interface Science, 2022, 608, 2921-2931.	5.0	30
3	Current advances on g-C3N4-based fluorescence detection for environmental contaminants. Journal of Hazardous Materials, 2022, 425, 127990.	6.5	26
4	Interlayer Modification Using Phenylethylamine Tetrafluoroborate for Highly Effective Perovskite Solar Cells. ACS Applied Energy Materials, 2022, 5, 658-666.	2.5	8
5	5â€Chloroindole as Interface Modifier to Improve the Efficiency and Stability of Planar Perovskite Solar Cells. Solar Rrl, 2022, 6, .	3.1	9
6	Improved visible-light activities of ultrathin CoPc/g-C3N4 heterojunctions by N-doped graphene modulation for selective benzyl alcohol oxidation. Materials Today Energy, 2022, 25, 100963.	2.5	11
7	Interface Modulation of FePc/Porous Ti(HPO ₄) ₂ Zâ€5cheme Heterojunctions with Ultrafine Ag for Efficiently Photocatalytic CO Oxidation. Small Structures, 2022, 3, .	6.9	9
8	Construction of 2D Zn-MOF/BiVO4 S-scheme heterojunction for efficient photocatalytic CO2 conversion under visible light irradiation. Chinese Journal of Catalysis, 2022, 43, 1331-1340.	6.9	55
9	Valence-mixed iron phthalocyanines/(1 0 0) Bi2MoO6 nanosheet Z-scheme heterojunction catalysts for efficient visible-light degradation of 2-chlorophenol via preferential dechlorination. Chemical Engineering Journal, 2022, 440, 135786.	6.6	17
10	Strategies and reaction systems for solar-driven CO2 reduction by water. , 2022, 1, 1.		10
11	Dual-metal Ni and Fe phthalocyanine/boron-doped g-C ₃ N ₄ <i>Z</i> -scheme 2D-heterojunctions for visible-light selective aerobic alcohol oxidation. Journal of Materials Chemistry A, 2022, 10, 12062-12069.	5.2	8
12	N-Rich Doped Anatase TiO2 with Smart Defect Engineering as Efficient Photocatalysts for Acetaldehyde Degradation. Nanomaterials, 2022, 12, 1564.	1.9	8
13	Synthesis of SnO2/rGO/g-C3N4 composite nanomaterials with efficient charge transfer for sensitive optoelectronic detection of NO2 gas. Materials Research Bulletin, 2022, 153, 111894.	2.7	8
14	Synergy of dual single Ni and Co atoms on borate modified g-C3N4 for photocatalytic CO2 reduction. Materials Research Bulletin, 2022, 153, 111883.	2.7	18
15	TiO ₂ -Modulated tetra(4-carboxyphenyl)porphyrin/perylene diimide organic Z-scheme nano-heterojunctions for efficient visible-light catalytic CO ₂ reduction. Nanoscale, 2022, 14, 8041-8049.	2.8	9
16	Synthesis of mixed-valence Cu phthalocyanine/graphene/g-C ₃ N ₄ ultrathin heterojunctions as efficient photocatalysts for CO ₂ reduction. Catalysis Science and Technology, 2022, 12, 4817-4825.	2.1	6
17	Improved Photocatalytic Activities of g-C ₃ N ₄ Nanosheets by B Doping and Ru-Oxo Cluster Modification for CO ₂ Conversion. Journal of Physical Chemistry C, 2022, 126, 9704-9712.	1.5	6
18	Porous two-dimension MnO2-C3N4/titanium phosphate nanocomposites as efficient photocatalsyts for CO oxidation and mechanisms. Applied Catalysis B: Environmental, 2021, 282, 119563.	10.8	25

#	Article	IF	CITATIONS
19	Synergetic Subnano Ni―and Mnâ€Oxo Clusters Anchored by Chitosan Oligomers on 2D gâ€C 3 N 4 Boost Photocatalytic CO 2 Reduction. Solar Rrl, 2021, 5, 2000472.	3.1	20
20	Au-Modulated Z-Scheme CuPc/BiVO ₄ Nanosheet Heterojunctions toward Efficient CO ₂ Conversion under Wide-Visible-Light Irradiation. ACS Sustainable Chemistry and Engineering, 2021, 9, 2400-2408.	3.2	20
21	Nitrate removal from low C/N wastewater at low temperature by immobilized Pseudomonas sp. Y39-6 with versatile nitrate metabolism pathways. Bioresource Technology, 2021, 326, 124794.	4.8	49
22	Recent advances in BiOBr-based photocatalysts for environmental remediation. Chinese Chemical Letters, 2021, 32, 3265-3276.	4.8	92
23	Controlled Synthesis of Nitro-Terminated Poly[2-(3-thienyl)-ethanol]/g-C ₃ N ₄ Nanosheet Heterojunctions for Efficient Visible-Light Photocatalytic Hydrogen Evolution. ACS Sustainable Chemistry and Engineering, 2021, 9, 7306-7317.	3.2	21
24	Controlled Construction of Copper Phthalocyanine/αâ€Fe ₂ O ₃ Ultrathin Sâ€Scheme Heterojunctions for Efficient Photocatalytic CO ₂ Reduction under Wide Visibleâ€Light Irradiation. Small Science, 2021, 1, 2100050.	5.8	34
25	Significantly Raised Visibleâ€Light Photocatalytic H ₂ Evolution on a 2D/2D ReS ₂ /In ₂ ZnS ₄ van der Waals Heterostructure. Small, 2021, 17, e2100296.	5.2	38
26	Energy Platform for Directed Charge Transfer in the Cascade Zâ€Scheme Heterojunction: CO ₂ Photoreduction without a Cocatalyst. Angewandte Chemie, 2021, 133, 21074-21082.	1.6	23
27	Significantly Raised Visibleâ€Light Photocatalytic H ₂ Evolution on a 2D/2D ReS ₂ /In ₂ ZnS ₄ van der Waals Heterostructure (Small 32/2021). Small, 2021, 17, 2170168.	5.2	1
28	Energy Platform for Directed Charge Transfer in the Cascade Zâ€Scheme Heterojunction: CO ₂ Photoreduction without a Cocatalyst. Angewandte Chemie - International Edition, 2021, 60, 20906-20914.	7.2	132
29	Construction of Sixâ€Oxygenâ€Coordinated Single Ni Sites on gâ€C ₃ N ₄ with Boronâ€Oxo Species for Photocatalytic Waterâ€Activationâ€Induced CO ₂ Reduction. Advanced Materials, 2021, 33, e2105482.	11.1	128
30	Efficient wide-spectrum photocatalytic overall water splitting over ultrathin molecular nickel phthalocyanine/BiVO4 Z-scheme heterojunctions without noble metals. Applied Catalysis B: Environmental, 2021, 295, 120260.	10.8	49
31	Improved photocatalytic activities of recyclable porous Fe2O3 nanotubes by modifying with nano-sized SiO2 and g-C3N4 for degrading 2-chlorophenol. Materials Research Bulletin, 2021, 142, 111416.	2.7	3
32	Ultrathin phosphate-modulated zinc phthalocyanine/perylenete diimide supermolecule Z-scheme heterojunctions as efficiently wide visible-light photocatalysts for CO2 conversion. Chemical Engineering Journal, 2021, 426, 131266.	6.6	20
33	Alkali Metal Fluoride-Modified Tin Oxide for n–i–p Planar Perovskite Solar Cells. ACS Applied Materials & Interfaces, 2021, 13, 50083-50092.	4.0	12
34	Graphene-Modulated PDI/g-C ₃ N ₄ All-Organic S-Scheme Heterojunction Photocatalysts for Efficient CO ₂ Reduction under Full-Spectrum Irradiation. Journal of Physical Chemistry C, 2021, 125, 23830-23839.	1.5	24
35	Improved photocatalytic activities of porous In2O3 with large surface area by coupling with K-modified CuO for degrading pollutants. Catalysis Today, 2020, 339, 403-410.	2.2	20
36	Efficiently photocatalytic degradation of monochlorophenol on in-situ fabricated BiPO4/Ĵ²-Bi2O3 heterojunction microspheres and O2-free hole-induced selective dechloridation conversion with H2 evolution. Applied Catalysis B: Environmental, 2020, 263, 118313.	10.8	42

#	Article	IF	CITATIONS
37	Improved visible-light activities of g-C3N4 nanosheets by co-modifying nano-sized SnO2 and Ag for CO2 reduction and 2,4-dichlorophenol degradation. Materials Research Bulletin, 2020, 122, 110676.	2.7	36
38	Construction of a triple sequential junction for efficient separation of photogenerated charges in photocatalysis. Chemical Communications, 2020, 56, 197-200.	2.2	11
39	The synthesis of porous ultrathin graphitic carbon nitride for the ultrasensitive fluorescence detection of 2,4,6-trinitrophenol in environmental water. Environmental Science: Nano, 2020, 7, 262-271.	2.2	28
40	Tailored elasticity combined with biomimetic surface promotes nanoparticle transcytosis to overcome mucosal epithelial barrier. Biomaterials, 2020, 262, 120323.	5.7	45
41	Atomic-Level Insights into the Edge Active ReS ₂ Ultrathin Nanosheets for High-Efficiency Light-to-Hydrogen Conversion. , 2020, 2, 1484-1494.		65
42	Efficient singlet oxygen generation by excitonic energy transfer on ultrathin g-C3N4 for selective photocatalytic oxidation of methyl-phenyl-sulfide with O2. Chinese Chemical Letters, 2020, 31, 2784-2788.	4.8	52
43	Improved Photocatalytic Activity of Porous In2O3 by co-Modifying Nanosized CuO and Ag with Synergistic Effects. Chemical Research in Chinese Universities, 2020, 36, 1116-1121.	1.3	7
44	Efficiently photocatalytic conversion of CO2 on ultrathin metal phthalocyanine/g-C3N4 heterojunctions by promoting charge transfer and CO2 activation. Applied Catalysis B: Environmental, 2020, 277, 119199.	10.8	84
45	Synthesis of nanosized Ag-modified 2D/2D hydroxylated g-C3N4/TS-1 Z-scheme nanocomposites for efficient photocatalytic CO2 reduction. Materials Research Bulletin, 2020, 130, 110926.	2.7	33
46	Actinyl-Modified g-C ₃ N ₄ as CO ₂ Activation Materials for Chemical Conversion and Environmental Remedy via an Artificial Photosynthetic Route. Inorganic Chemistry, 2020, 59, 8369-8379.	1.9	8
47	Highly sensitive fluorescence detection of chloride ion in aqueous solution with Ag-modified porous g-C3N4 nanosheets. Chinese Chemical Letters, 2020, 31, 2725-2729.	4.8	26
48	Ultrafine SnO ₂ /010 Facet-Exposed BiVO ₄ Nanocomposites as Efficient Photoanodes for Controllable Conversion of 2,4-Dichlorophenol via a Preferential Dechlorination Path. ACS Applied Materials & Interfaces, 2020, 12, 28264-28272.	4.0	19
49	Synthesis of SnO2/yolk-shell LaFeO3 nanocomposites as efficient visible-light photocatalysts for 2,4-dichlorophenol degradation. Materials Research Bulletin, 2020, 127, 110857.	2.7	47
50	Graphene-modulated assembly of zinc phthalocyanine on BiVO ₄ nanosheets for efficient visible-light catalytic conversion of CO ₂ . Chemical Communications, 2020, 56, 4926-4929.	2.2	17
51	Mgâ^'Oâ€Bridged Polypyrrole/g ₃ N ₄ Nanocomposites as Efficient Visibleâ€Light Catalysts for Hydrogen Evolution. ChemSusChem, 2020, 13, 3707-3717.	3.6	19
52	Ultrathin Phosphateâ€Modulated Co Phthalocyanine/g ₃ N ₄ Heterojunction Photocatalysts with Single Co–N ₄ (II) Sites for Efficient O ₂ Activation. Advanced Science, 2020, 7, 2001543.	5.6	99
53	Controlled synthesis of novel Z-scheme iron phthalocyanine/porous WO3 nanocomposites as efficient photocatalysts for CO2 reduction. Applied Catalysis B: Environmental, 2020, 270, 118849.	10.8	83
54	Synthesis of Ni2+ cation modified TS-1 molecular sieve nanosheets as effective photocatalysts for alcohol oxidation and pollutant degradation. Chinese Journal of Catalysis, 2020, 41, 1589-1602.	6.9	29

#	Article	IF	CITATIONS
55	The synthesis of interface-modulated ultrathin Ni(<scp>ii</scp>) MOF/g-C ₃ N ₄ heterojunctions as efficient photocatalysts for CO ₂ reduction. Nanoscale, 2020, 12, 10010-10018.	2.8	64
56	Innentitelbild: Dimensionâ€Matched Zinc Phthalocyanine/BiVO ₄ Ultrathin Nanocomposites for CO ₂ Reduction as Efficient Wideâ€Visibleâ€Lightâ€Driven Photocatalysts via a Cascade Charge Transfer (Angew. Chem. 32/2019). Angewandte Chemie, 2019, 131, 10878-10878.	1.6	0
57	Improved Photoactivities of Largeâ€surfaceâ€area gâ€C ₃ N ₄ for CO ₂ Conversion by Controllably Introducing Coâ€and Niâ€Species to Effectively Modulate Photogenerated Charges. ChemCatChem, 2019, 11, 6282-6287.	1.8	15
58	Review on Photogenerated Hole Modulation Strategies in Photoelectrocatalysis for Solar Fuel Production. ChemCatChem, 2019, 11, 5875-5884.	1.8	17
59	Dimensionâ€Matched Zinc Phthalocyanine/BiVO ₄ Ultrathin Nanocomposites for CO ₂ Reduction as Efficient Wideâ€Visibleâ€Lightâ€Driven Photocatalysts via a Cascade Charge Transfer. Angewandte Chemie, 2019, 131, 10989-10994.	1.6	44
60	Surface co-modification with highly-dispersed Mn & Cu oxides of g-C3N4 nanosheets for efficiently photocatalytic reduction of CO2 to CO and CH4. Applied Surface Science, 2019, 492, 125-134.	3.1	51
61	Improved photoactivities for CO2 conversion and phenol degradation of α-Fe2O3 nanoparticles by co-coupling nano-sized BiPO4 and CuO to modulate electrons. Journal of Alloys and Compounds, 2019, 800, 231-239.	2.8	17
62	Dimensionâ€Matched Zinc Phthalocyanine/BiVO ₄ Ultrathin Nanocomposites for CO ₂ Reduction as Efficient Wideâ€Visibleâ€Lightâ€Driven Photocatalysts via a Cascade Charge Transfer. Angewandte Chemie - International Edition, 2019, 58, 10873-10878.	7.2	168
63	Atomically Dispersed Single Co Sites in Zeolitic Imidazole Frameworks Promoting Highâ€Efficiency Visibleâ€Lightâ€Driven Hydrogen Production. Chemistry - A European Journal, 2019, 25, 9670-9677.	1.7	10
64	Improved visible-light photoactivities of porous LaFeO ₃ by coupling with nanosized alkaline earth metal oxides and mechanism insight. Catalysis Science and Technology, 2019, 9, 3149-3157.	2.1	40
65	Promoted oxygen activation of layered micro-mesoporous structured titanium phosphate nanoplates by coupling nano-sized Î-MnO2 with surface pits for efficient photocatalytic oxidation of CO. Applied Catalysis B: Environmental, 2019, 254, 260-269.	10.8	33
66	Synthesis of activated carbon-supported TiO2-based nano-photocatalysts with well recycling for efficiently degrading high-concentration pollutants. Catalysis Today, 2019, 335, 557-564.	2.2	64
67	A two-dimensional metal–organic framework accelerating visible-light-driven H ₂ production. Nanoscale, 2019, 11, 8304-8309.	2.8	26
68	Synthesis of Si–O-Bridged <i>g</i> -C ₃ N ₄ /WO ₃ 2D-Heterojunctional Nanocomposites as Efficient Photocatalysts for Aerobic Alcohol Oxidation and Mechanism Insight. ACS Sustainable Chemistry and Engineering, 2019, 7, 9916-9927.	3.2	44
69	Review of strategies for the fabrication of heterojunctional nanocomposites as efficient visible-light catalysts by modulating excited electrons with appropriate thermodynamic energy. Journal of Materials Chemistry A, 2019, 7, 10879-10897.	5.2	98
70	CO ₂ Photoreduction: Heterostructure Engineering of a Reverse Water Gas Shift Photocatalyst (Adv. Sci. 22/2019). Advanced Science, 2019, 6, 1970134.	5.6	3
71	Synthesis of Au-decorated three-phase-mixed TiO ₂ /phosphate modified active carbon nanocomposites as easily-recycled efficient photocatalysts for degrading high-concentration 2,4-DCP. RSC Advances, 2019, 9, 38414-38421.	1.7	9
72	Improved photoelectric properties of BiOBr nanoplates by co-modifying SnO2 and Ag to promote photoelectrons trapped by adsorbed O2. Science China Materials, 2019, 62, 653-661.	3.5	9

#	Article	IF	CITATIONS
73	Synthesis of SPR Au/BiVO4 quantum dot/rutile-TiO2 nanorod array composites as efficient visible-light photocatalysts to convert CO2 and mechanism insight. Applied Catalysis B: Environmental, 2019, 244, 641-649.	10.8	94
74	Improved fluorescence test of chromium (VI) in aqueous solution with g-C3N4 nanosheet and mechanisms. Materials Research Bulletin, 2019, 112, 9-15.	2.7	15
75	Synthesis of g-C3N4-based photocatalysts with recyclable feature for efficient 2,4-dichlorophenol degradation and mechanisms. Applied Catalysis B: Environmental, 2019, 243, 57-65.	10.8	100
76	Improved visible-light photoactivity of Pt/g-C3N4 nanosheets for solar fuel production via pretreated boric acid modification. Research on Chemical Intermediates, 2019, 45, 249-259.	1.3	16
77	Visible-light induced electron modulation to improve photoactivities of coral-like Bi2WO6 by coupling SnO2 as a proper energy platform. Catalysis Today, 2019, 327, 288-294.	2.2	11
78	2D Metal Organic Framework Nanosheet: A Universal Platform Promoting Highly Efficient Visible‣ightâ€Induced Hydrogen Production. Advanced Energy Materials, 2019, 9, 1803402.	10.2	200
79	Synthesis of ZnO/Bi-doped porous LaFeO3 nanocomposites as highly efficient nano-photocatalysts dependent on the enhanced utilization of visible-light-excited electrons. Applied Catalysis B: Environmental, 2018, 231, 23-33.	10.8	113
80	Single-crystal TiO2 nanorods assembly for efficient and stable cocatalyst-free photocatalytic hydrogen evolution. Applied Catalysis B: Environmental, 2018, 229, 1-7.	10.8	82
81	Improved visible-light activities of nanocrystalline CdS by coupling with ultrafine NbN with lattice matching for hydrogen evolution. Sustainable Energy and Fuels, 2018, 2, 549-552.	2.5	35
82	Synthesis of Silicateâ€Bridged Heterojunctional SnO ₂ /BiVO ₄ Nanoplates as Efficient Photocatalysts to Convert CO ₂ and Degrade 2,4â€Dichlorophenol. Particle and Particle Systems Characterization, 2018, 35, 1700320.	1.2	13
83	Synthesis of nano SnO2-coupled mesoporous molecular sieve titanium phosphate as a recyclable photocatalyst for efficient decomposition of 2,4-dichlorophenol. Nano Research, 2018, 11, 1612-1624.	5.8	37
84	Synthesis of Large Surfaceâ€Area gâ€C ₃ N ₄ Comodified with MnO <i>_x</i> and Auâ€TiO ₂ as Efficient Visibleâ€Light Photocatalysts for Fuel Production. Advanced Energy Materials, 2018, 8, 1701580.	10.2	157
85	Exceptional photocatalytic activities for CO2 conversion on Al O bridged g-C3N4/α-Fe2O3 z-scheme nanocomposites and mechanism insight with isotopesZ. Applied Catalysis B: Environmental, 2018, 221, 459-466.	10.8	154
86	Improved visible-light activities for degrading pollutants on TiO2/g-C3N4 nanocomposites by decorating SPR Au nanoparticles and 2,4-dichlorophenol decomposition path. Journal of Hazardous Materials, 2018, 342, 715-723.	6.5	190
87	Metallic MoN ultrathin nanosheets boosting high performance photocatalytic H ₂ production. Journal of Materials Chemistry A, 2018, 6, 23278-23282.	5.2	37
88	Improved Visible-Light Activities of Rutile Nanorod by Comodifying Highly Dispersed Surface Plasmon Resonance Au Nanoparticles and HF Groups for Aerobic Selective Alcohol Oxidation. ACS Sustainable Chemistry and Engineering, 2018, 6, 14652-14659.	3.2	14
89	Dimension-matched plasmonic Au/TiO ₂ /BiVO ₄ nanocomposites as efficient wide-visible-light photocatalysts to convert CO ₂ and mechanistic insights. Journal of Materials Chemistry A, 2018, 6, 11838-11845.	5.2	72
90	Exceptional visible-light activities of g-C3N4 nanosheets dependent on the unexpected synergistic effects of prolonging charge lifetime and catalyzing H2 evolution with H2O. Applied Catalysis B: Environmental, 2018, 237, 50-58.	10.8	51

#	Article	IF	CITATIONS
91	Prolonged lifetime and enhanced separation of photogenerated charges of nanosized α-Fe2O3 by coupling SnO2 for efficient visible-light photocatalysis to convert CO2 and degrade acetaldehyde. Nano Research, 2017, 10, 2321-2331.	5.8	44
92	Photogenerated electron modulation to dominantly induce efficient 2,4-dichlorophenol degradation on BiOBr nanoplates with different phosphate modification. Applied Catalysis B: Environmental, 2017, 209, 320-328.	10.8	91
93	Efficient photodecomposition of 2,4-dichlorophenol on recyclable phase-mixed hierarchically structured Bi ₂ O ₃ coupled with phosphate-bridged nano-SnO ₂ . Environmental Science: Nano, 2017, 4, 1147-1154.	2.2	37
94	Enhanced photocatalytic activities of commercial P25 TiO 2 by trapping holes and transferring electrons for CO 2 conversion and 2,4-dichlorophenol degradation. Materials Research Bulletin, 2017, 92, 23-28.	2.7	21
95	Enhanced photoelectrochemical activities for water oxidation and phenol degradation on WO3 nanoplates by transferring electrons and trapping holes. Scientific Reports, 2017, 7, 1303.	1.6	23
96	Effect of Ni doping in Ni _x Mn _{1â^'x} Ti ₁₀ (x = 0.1–0.5) on activity and SO ₂ resistance for NH ₃ -SCR of NO studied with in situ DRIFTS. Catalysis Science and Technology, 2017, 7, 3243-3257.	2.1	111
97	Improved photocatalytic activities of g-C3N4 nanosheets by effectively trapping holes with halogen-induced surface polarization and 2,4-dichlorophenol decomposition mechanism. Applied Catalysis B: Environmental, 2017, 218, 60-67.	10.8	123
98	Synthesis of TiO2/g-C3N4 nanocomposites with phosphate–oxygen functional bridges for improved photocatalytic activity. Chinese Journal of Catalysis, 2017, 38, 1072-1078.	6.9	45
99	Surface-engineering strategies for g-C3N4 as efficient visible-light photocatalyst. Current Opinion in Green and Sustainable Chemistry, 2017, 6, 57-62.	3.2	19
100	Synthesis of MnNi–SAPO-34 by a one-pot hydrothermal method and its excellent performance for the selective catalytic reduction of NO by NH ₃ . Catalysis Science and Technology, 2017, 7, 4984-4995.	2.1	31
101	A self-supporting bimetallic Au@Pt core-shell nanoparticle electrocatalyst for the synergistic enhancement of methanol oxidation. Scientific Reports, 2017, 7, 6347.	1.6	56
102	Improved photoelectrocatalytic activities of BiOCl with high stability for water oxidation and MO degradation by coupling RGO and modifying phosphate groups to prolong carrier lifetime. Applied Catalysis B: Environmental, 2017, 203, 355-362.	10.8	107
103	Synthesis of SnO2/B-P codoped g-C3N4 nanocomposites as efficient cocatalyst-free visible-light photocatalysts for CO2 conversion and pollutant degradation. Applied Catalysis B: Environmental, 2017, 201, 486-494.	10.8	254
104	Facile Synthesis of Vanadium Oxide/Reduced Graphene Oxide Composite Catalysts for Enhanced Hydroxylation of Benzene to Phenol. Catalysts, 2016, 6, 74.	1.6	30
105	Coupling of Nanocrystalline Anatase TiO2 to Porous Nanosized LaFeO3 for Efficient Visible-Light Photocatalytic Degradation of Pollutants. Nanomaterials, 2016, 6, 22.	1.9	35
106	Selective Oxidation of Aliphatic Alcohols using Molecular Oxygen at Ambient Temperature: Mixed-Valence Vanadium Oxide Photocatalysts. ACS Catalysis, 2016, 6, 3580-3588.	5.5	76
107	Exceptional Visibleâ€Lightâ€Driven Cocatalystâ€Free Photocatalytic Activity of gâ€C ₃ N ₄ by Well Designed Nanocomposites with Plasmonic Au and SnO ₂ . Advanced Energy Materials, 2016, 6, 1601190.	10.2	207
108	Exceptional Visible-Light Activities of TiO ₂ -Coupled N-Doped Porous Perovskite LaFeO ₃ for 2,4-Dichlorophenol Decomposition and CO ₂ Conversion. Environmental Science & Technology, 2016, 50, 13600-13610.	4.6	146

Liqiang Jing

#	Article	IF	CITATIONS
109	The effects of BaO on the catalytic activity of La1.6Ba0.4NiO4 in direct decomposition of NO. Journal of Molecular Catalysis A, 2016, 423, 277-284.	4.8	18
110	Soot Combustion over Nanostructured Ceria with Different Morphologies. Scientific Reports, 2016, 6, 29062.	1.6	56
111	Exceptional performance of photoelectrochemical water oxidation of single-crystal rutile TiO2 nanorods dependent on the hole trapping of modified chloride. Scientific Reports, 2016, 6, 21430.	1.6	30
112	Accepting Excited High-Energy-Level Electrons and Catalyzing H ₂ Evolution of Dual-Functional Ag-TiO ₂ Modifier for Promoting Visible-Light Photocatalytic Activities of Nanosized Oxides. Journal of Physical Chemistry C, 2016, 120, 11831-11836.	1.5	27
113	Enhanced Cocatalyst-Free Visible-Light Activities for Photocatalytic Fuel Production of g-C ₃ N ₄ by Trapping Holes and Transferring Electrons. Journal of Physical Chemistry C, 2016, 120, 98-107.	1.5	135
114	Enhanced charge separation of rutile TiO ₂ nanorods by trapping holes and transferring electrons for efficient cocatalyst-free photocatalytic conversion of CO ₂ to fuels. Chemical Communications, 2016, 52, 5027-5029.	2.2	45
115	Enhanced visible-light activities of porous BiFeO3 by coupling with nanocrystalline TiO2 and mechanism. Applied Catalysis B: Environmental, 2016, 180, 219-226.	10.8	223
116	Activity and SO ₂ resistance of amorphous Ce _a TiO _x catalysts for the selective catalytic reduction of NO with NH ₃ : in situ DRIFT studies. Catalysis Science and Technology, 2016, 6, 7151-7162.	2.1	98
117	Enhanced photocatalytic activity of Cl-residual rutile TiO ₂ nanorods after targeted co-modification with phosphoric and boric acids. Physical Chemistry Chemical Physics, 2015, 17, 15837-15842.	1.3	18
118	Synthesis of TiO2/g-C3N4 nanocomposites as efficient photocatalysts dependent on the enhanced photogenerated charge separation. Materials Research Bulletin, 2015, 70, 494-499.	2.7	75
119	Phosphate-bridged TiO2–BiVO4 nanocomposites with exceptional visible activities for photocatalytic water splitting. Journal of Alloys and Compounds, 2015, 631, 120-124.	2.8	74
120	The promotion effect of surface negative electrostatic field on the photogenerated charge separation of BiVO ₄ and its contribution to the enhanced PEC water oxidation. Chemical Communications, 2015, 51, 2821-2823.	2.2	42
121	ZnO-dotted porous ZnS cluster microspheres for high efficient, Pt-free photocatalytic hydrogen evolution. Scientific Reports, 2015, 5, 8858.	1.6	34
122	Enhanced visible-light activities for PEC water reduction of CuO nanoplates by coupling with anatase TiO2 and mechanism. Applied Surface Science, 2015, 351, 681-685.	3.1	25
123	Physicochemical properties and photocatalytic activity of H3PW12O40/TiO2. Kinetics and Catalysis, 2015, 56, 308-315.	0.3	10
124	Synthesis of silicate-bridged ZnO/g-C ₃ N ₄ nanocomposites as efficient photocatalysts and its mechanism. RSC Advances, 2015, 5, 37275-37280.	1.7	40
125	Modification Strategies with Inorganic Acids for Efficient Photocatalysts by Promoting the Adsorption of O ₂ . ACS Applied Materials & amp; Interfaces, 2015, 7, 22727-22740.	4.0	68
126	Role of quaternary N in N-doped graphene–Fe ₂ O ₃ nanocomposites as efficient photocatalysts for CO ₂ reduction and acetaldehyde degradation. RSC Advances, 2015, 5, 85061-85064.	1.7	27

#	Article	IF	CITATIONS
127	Detection of NOx down to ppb levels at room temperature based on highly mesoporous hierarchical Ni(OH)2–In(OH)3 double hydroxide composites. Journal of Materials Science: Materials in Electronics, 2015, 26, 6612-6624.	1.1	10
128	Enhanced photocatalytic activity for degrading pollutants of g-C3N4 by promoting oxygen adsorption after H3BO3 modification. Applied Surface Science, 2015, 358, 240-245.	3.1	21
129	Improved photoactivity of TiO ₂ –Fe ₂ O ₃ nanocomposites for visible-light water splitting after phosphate bridging and its mechanism. Physical Chemistry Chemical Physics, 2015, 17, 5043-5050.	1.3	84
130	Enhanced Photocatalytic Activity of P25 TiO ₂ after Modification with Phosphateâ€Treated Porous SiO ₂ . ChemPlusChem, 2014, 79, 1271-1277.	1.3	6
131	Facile Synthesis of Nâ€doped TiO ₂ and Its Enhanced Photocatalytic Activity for Degrading Colorless Pollutants. ChemPlusChem, 2014, 79, 737-742.	1.3	16
132	Effects of Inorganic Acid Modification on Photocatalytic Performance of TiO ₂ and Its Activityâ€Enhanced Mechanism Related to Adsorbed O ₂ . ChemPlusChem, 2014, 79, 318-324.	1.3	13
133	Synthesis of long-lived photogenerated charge carriers of Si-modified α-Fe2O3 and its enhanced visible photocatalytic activity. Materials Research Bulletin, 2014, 49, 331-337.	2.7	11
134	Phosphate-modified graphitic C3N4 as efficient photocatalyst for degrading colorless pollutants by promoting O2 adsorption. Chemical Communications, 2014, 50, 1999.	2.2	89
135	Synthesis of mesoporous TiO ₂ -coupled Fe ₂ O ₃ as efficient visible nano-photocatalysts for degrading colorless pollutants. RSC Advances, 2014, 4, 52053-52059.	1.7	17
136	Effective Visible-Excited Charge Separation in Silicate-Bridged ZnO/BiVO ₄ Nanocomposite and Its Contribution to Enhanced Photocatalytic Activity. ACS Applied Materials & Interfaces, 2014, 6, 18550-18557.	4.0	79
137	Highly mesoporous hierarchical nickel and cobalt double hydroxide composite: fabrication, characterization and ultrafast NOx gas sensors at room temperature. Journal of Materials Chemistry A, 2014, 2, 4961.	5.2	74
138	Capturing photogenerated electrons and holes at the B/Cl co-modified rutile TiO ₂ nanorods during organic pollutant degradation. RSC Advances, 2014, 4, 29964.	1.7	13
139	Heterostructured Co3O4/PEl–CNTs composite: fabrication, characterization and CO gas sensors at room temperature. Journal of Materials Chemistry A, 2014, 2, 4558-4565.	5.2	49
140	Enhanced Visible Activities of α-Fe ₂ O ₃ by Coupling N-Doped Graphene and Mechanism Insight. ACS Catalysis, 2014, 4, 990-998.	5.5	132
141	Electrospinning of mesoporous p-type ln ₂ O ₃ /TiO ₂ composite nanofibers for enhancing NO _x gas sensing properties at room temperature. CrystEngComm, 2014, 16, 9116-9124.	1.3	41
142	One-step synthesis of mesoporous Al ₂ O ₃ –In ₂ O ₃ nanofibres with remarkable gas-sensing performance to NO _x at room temperature. Journal of Materials Chemistry A, 2014, 2, 949-956.	5.2	84
143	Long-lived photogenerated charge carriers of 001-facet-exposed TiO2 with enhanced thermal stability as an efficient photocatalyst. Applied Catalysis B: Environmental, 2014, 147, 29-34.	10.8	44
144	Longâ€Lived, Visibleâ€Lightâ€Excited Charge Carriers of TiO ₂ /BiVO ₄ Nanocomposites and their Unexpected Photoactivity for Water Splitting, Advanced Energy Materials, 2014, 4, 1300995	10.2	268

#	Article	IF	CITATIONS
145	Effective charge separation in the rutile TiO2 nanorod-coupled α-Fe2O3 with exceptionally high visible activities. Scientific Reports, 2014, 4, 6180.	1.6	95
146	Enhancement Effects of Cobalt Phosphate Modification on Activity for Photoelectrochemical Water Oxidation of TiO ₂ and Mechanism Insights. ACS Applied Materials & Interfaces, 2013, 5, 4046-4052.	4.0	56
147	Surface tuning for oxide-based nanomaterials as efficient photocatalysts. Chemical Society Reviews, 2013, 42, 9509.	18.7	564
148	Growth and characterization of BCN nanotubes with high boron and nitrogen content. Journal of Chemical Sciences, 2013, 125, 1169-1176.	0.7	8
149	Facile Synthesis of Surface-Modified Nanosized α-Fe ₂ O ₃ as Efficient Visible Photocatalysts and Mechanism Insight. Journal of Physical Chemistry C, 2013, 117, 1358-1365.	1.5	77
150	Exceptional Photocatalytic Activity of 001-Facet-Exposed TiO ₂ Mainly Depending on Enhanced Adsorbed Oxygen by Residual Hydrogen Fluoride. ACS Catalysis, 2013, 3, 1378-1385.	5.5	137
151	Facile Synthesis of Phosphateâ€Functionalized MWCNT–TiO ₂ Nanocomposites as Efficient Photocatalysts and Insights into the Roles of Nanostructured Carbon. ChemPlusChem, 2013, 78, 670-676.	1.3	7
152	Enhanced visible photocatalytic activity of nanocrystalline α-Fe2O3 by coupling phosphate-functionalized graphene. RSC Advances, 2013, 3, 7438.	1.7	31
153	Enhanced photocatalytic activity of nc-TiO2 by promoting photogenerated electrons captured by the adsorbed oxygen. Physical Chemistry Chemical Physics, 2012, 14, 8530.	1.3	73
154	Acceleration effects of phosphate modification on the decay dynamics of photo-generated electrons of TiO2 and its photocatalytic activity. Chemical Communications, 2012, 48, 10775.	2.2	58
155	Synthesis of efficient TiO2-based photocatalysts by phosphate surface modification and the activity-enhanced mechanisms. Applied Surface Science, 2012, 258, 3340-3349.	3.1	21
156	Facile fabrication of efficient AgBr–TiO2 nanoheterostructured photocatalyst for degrading pollutants and its photogenerated charge transfer mechanism. Journal of Hazardous Materials, 2012, 243, 169-178.	6.5	62
157	Controllable synthesis of floatable nanocrystalline Ag2S and Ag by a silane coupling agent-modified solvothermal method. Materials Research Bulletin, 2012, 47, 3732-3737.	2.7	9
158	Synthesis of efficient N-containing TiO2photocatalysts with high anatase thermal stability and the effects of the nitrogen residue on the photoinduced charge separation. Physical Chemistry Chemical Physics, 2012, 14, 1352-1359.	1.3	30
159	Dynamics of photogenerated charges in the phosphate modified TiO2 and the enhanced activity for photoelectrochemical water splitting. Energy and Environmental Science, 2012, 5, 6552.	15.6	143
160	Synthesis of Efficient Nanosized Rutile TiO ₂ and Its Main Factors Determining Its Photodegradation Activity: Roles of Residual Chloride and Adsorbed Oxygen. Journal of Physical Chemistry C, 2012, 116, 17094-17100.	1.5	47
161	Synthesis of High-Activity TiO ₂ -Based Photocatalysts by Compounding a Small Amount of Porous Nanosized LaFeO ₃ and the Activity-Enhanced Mechanisms. Journal of Physical Chemistry C, 2011, 115, 12375-12380.	1.5	62
162	Synthesis of large surface area nano-sized BiVO4 by an EDTA-modified hydrothermal process and its enhanced visible photocatalytic activity. Journal of Solid State Chemistry, 2011, 184, 3050-3054.	1.4	57

#	Article	IF	CITATIONS
163	Synthesis of nanocrystalline anatase TiO2 by one-pot two-phase separated hydrolysis-solvothermal processes and its high activity for photocatalytic degradation of rhodamine B. Journal of Hazardous Materials, 2010, 176, 139-145.	6.5	87
164	Electrochemical deposition of nano-structured ZnO on the nanocrystalline TiO2 film and its characterization. Science China Chemistry, 2010, 53, 1732-1736.	4.2	6
165	Synthesis of large surface area LaFeO3 nanoparticles by SBA-16 template method as high active visible photocatalysts. Journal of Nanoparticle Research, 2010, 12, 967-974.	0.8	112
166	Effects of the co-addition of Zn2+ and sodium dodecylbenzenesulfonate on photocatalytic activity and wetting performance of anatase TiO2 nanoparticle films. Thin Solid Films, 2010, 518, 3177-3181.	0.8	11
167	Surface modification of nanocrystalline anatase with CTAB in the acidic condition and its effects on photocatalytic activity and preferential growth of TiO2. Applied Surface Science, 2010, 257, 151-156.	3.1	44
168	Effects of surface-modification with Bi2O3 on the thermal stability and photoinduced charge property of nanocrystalline anatase TiO2 and its enhanced photocatalytic activity. Applied Surface Science, 2009, 256, 657-663.	3.1	59
169	Enhanced photocatalytic activity for degrading Rhodamine B solution of commercial Degussa P25 TiO2 and its mechanisms. Journal of Hazardous Materials, 2009, 172, 1168-1174.	6.5	126
170	Controllable vertical growth onto anatase TiO2 nanoparticle films of ZnO nanorod arrays and their photoluminescence and superhydrophilic characteristics. Journal of Physics and Chemistry of Solids, 2009, 70, 867-873.	1.9	13
171	Catalytic Hydrogenation of Aqueous Nitrate over Pdâ^'Cu/ZrO ₂ Catalysts. Industrial & Engineering Chemistry Research, 2009, 48, 8356-8363.	1.8	36
172	Mesoporous SiO ₂ -Modified Nanocrystalline TiO ₂ with High Anatase Thermal Stability and Large Surface Area as Efficient Photocatalyst. Journal of Physical Chemistry C, 2009, 113, 1006-1013.	1.5	117
173	Preparation of Porous SiO ₂ -TiO ₂ Nanocomposites and Their Photocatalytic Activity. Wuji Cailiao Xuebao/Journal of Inorganic Materials, 2009, 24, 229-233.	0.6	1
174	Enhanced activity of bismuth-compounded TiO2 nanoparticles for photocatalytically degrading rhodamine B solution. Journal of Hazardous Materials, 2008, 160, 208-212.	6.5	54
175	Investigation on the electron transfer between anatase and rutile in nano-sized TiO2 by means of surface photovoltage technique and its effects on the photocatalytic activity. Solar Energy Materials and Solar Cells, 2008, 92, 1030-1036.	3.0	104
176	Superhydrophilic anatase TiO2 film with the micro- and nanometer-scale hierarchical surface structure. Materials Letters, 2008, 62, 3503-3505.	1.3	53
177	Preparation and Characterization of Stable Biphase TiO ₂ Photocatalyst with High Crystallinity, Large Surface Area, and Enhanced Photoactivity. Journal of Physical Chemistry C, 2008, 112, 3083-3089.	1.5	288
178	Photoinduced charge property of nanosized perovskite-type LaFeO3 and its relationships with photocatalytic activity under visible irradiation. Materials Research Bulletin, 2007, 42, 203-212.	2.7	162
179	Effects of Surface Oxygen Vacancies on Photophysical and Photochemical Processes of Zn-Doped TiO2Nanoparticles and Their Relationships. Journal of Physical Chemistry B, 2006, 110, 17860-17865.	1.2	397
180	Effects of doping La and Cu on photoinduced charge properties of TiO2 and its relationships with photocatalytic activity. Science in China Series B: Chemistry, 2006, 49, 345-350.	0.8	3

#	Article	IF	CITATIONS
181	Relationships of surface oxygen vacancies with photoluminescence and photocatalytic performance of ZnO nanoparticles. Science in China Series B: Chemistry, 2005, 48, 25-30.	0.8	79
182	Relationships of surface oxygen vacancies with photoluminescence and photocatalytic performance of ZnO nanoparticles. Science in China Series B: Chemistry, 2005, 48, 25.	0.8	8
183	The preparation and characterization of ZnO ultrafine particles. Materials Science & Engineering A: Structural Materials: Properties, Microstructure and Processing, 2002, 332, 356-361.	2.6	166
184	The surface properties and photocatalytic activities of ZnO ultrafine particles. Applied Surface Science, 2001, 180, 308-314.	3.1	317
185	Effect of biocides on the precipitation of calcium fluoride in the presence of anionic copolymeric inhibitors. Toxicological and Environmental Chemistry, 0, , 1-11.	0.6	1